

# Mass signature of supernova $\nu_\mu$ and $\nu_\tau$ neutrinos in SuperKamiokande

J. F. Beacom\* and P. Vogel†

*Department of Physics, California Institute of Technology  
Pasadena, CA 91125, USA*

(February 25, 1998)

The  $\nu_\mu$  and  $\nu_\tau$  neutrinos (and their antiparticles) from a Galactic core-collapse supernova can be observed in a water-Čerenkov detector by the neutral-current excitation of  $^{16}\text{O}$ . The number of events expected is several times greater than from neutral-current scattering on electrons. The observation of this signal would be a strong test that these neutrinos are produced in core-collapse supernovae, and with the right characteristics. In this paper, this signal is used as the basis for a technique of neutrino mass determination from a future Galactic supernova. The masses of the  $\nu_\mu$  and  $\nu_\tau$  neutrinos can either be measured or limited by their delay relative to the  $\bar{\nu}_e$  neutrinos. By comparing to the high-statistics  $\bar{\nu}_e$  data instead of the theoretical expectation, much of the model dependence is canceled. Numerical results are presented for a future supernova at 10 kpc as seen in the SuperKamiokande detector. Under reasonable assumptions, and in the presence of the expected counting statistics,  $\nu_\mu$  and  $\nu_\tau$  masses down to about 50 eV can be simply and robustly determined. The signal used here is more sensitive to small neutrino masses than the signal based on neutrino-electron scattering.

14.60.Pq, 97.60.Bw, 25.30.Pt, 95.55.Vj

## I. INTRODUCTION

When the core of a large star ( $M \geq 8M_\odot$ ) runs out of nuclear fuel, it collapses and forms a proto-neutron star with a central density well above the normal nuclear density (for a review of type-II supernova theory, see Ref. [1]). The total energy released in the collapse, i.e., the gravitational binding energy of the core ( $E_B \sim G_N M_\odot^2 / R$  with  $R \sim 10$  km), is about  $3 \times 10^{53}$  ergs; about 99% of that is carried away by neutrinos and antineutrinos, the particles with the longest mean free path. The proto-neutron star is dense enough that neutrinos diffuse outward over a timescale of several seconds, maintaining thermal equilibrium with the matter. When they are within about one mean free path of the edge, they escape freely, with a thermal spectrum characteristic of the surface of last scattering. The luminosities of the different neutrino flavors are approximately equal.

Those flavors which interact the most with the matter will decouple at the largest radius and thus the lowest temperature. The  $\nu_\mu$  and  $\nu_\tau$  neutrinos and their antiparticles, which we collectively call  $\nu_x$  neutrinos, have only neutral-current interactions with the matter, and therefore leave with the highest temperature, about 8 MeV (or  $\langle E \rangle \simeq 25$  MeV). The  $\bar{\nu}_e$  and  $\nu_e$  neutrinos have also charged-current interactions, and so leave with lower temperatures, about 5 MeV ( $\langle E \rangle \simeq 16$  MeV) and 3.5 MeV ( $\langle E \rangle \simeq 11$  MeV), respectively. The  $\nu_e$  temperature is lower because the material is neutron-rich and thus the  $\nu_e$  interact more than the  $\bar{\nu}_e$ . The observation of supernova  $\nu_x$  neutrinos would allow the details of the picture above to be tested. For a detailed description of the supernova neutrino emission, including the justification of our choice of temperatures, see Refs. [2,3].

Even after many decades of experiments, it is still not known whether neutrinos have mass. Results from several experiments strongly suggest that neutrino flavor mixing occurs in solar, atmospheric, and accelerator neutrinos, and proof of mixing would be a proof of mass. The requirement that neutrinos do not overclose the universe gives a bound for the sum of masses of stable neutrinos (see [4] and references therein):

$$\sum_{i=1}^3 m_{\nu_i} \lesssim 100 \text{ eV}. \quad (1)$$

However, direct kinematic tests of neutrino mass currently give limits for the masses compatible with the above cosmological bound only for the electron neutrino,  $m_{\bar{\nu}_e} \lesssim 5$  eV [5]. For the  $\nu_\mu$  and  $\nu_\tau$  neutrinos the kinematic limits far exceed the cosmological bound:  $m_{\nu_\mu} < 170$  keV [6], and  $m_{\nu_\tau} < 24$  MeV [6]. It is very unlikely that direct kinematic tests can improve these mass limits by the necessary orders of magnitude any time soon.

As we will show in detail below, the most promising method for determining these masses is with supernova neutrinos. Even a tiny mass will make the velocity slightly less than for a massless neutrino, and over the large distance to a supernova will cause a measurable delay in the arrival time. A neutrino with a mass  $m$  (in eV) and energy  $E$  (in MeV) will experience an energy-dependent delay (in s) relative to a massless neutrino in traveling over a distance  $D$  (in 10 kpc) of

$$\Delta t(E) = 0.515 \left( \frac{m}{E} \right)^2 D, \quad (2)$$

where only the lowest order in the small mass has been kept. Since one expects one type-II supernova about

every 30 years in our Galaxy [7], and since supernova neutrino detectors are currently operating, it is worthwhile to consider whether mass limits (or values) for  $\nu_x$  compatible with the cosmological bound, Eq. (1), can be obtained.

The problem of  $\nu_x$  mass determination with supernova neutrinos in existing (e.g., Refs. [8–12]) and proposed detectors (e.g., Refs. [13–15]) has been considered before. The present work differs from the previous ones by the method with which the  $\nu_x$  are detected: inelastic scattering on  $^{16}\text{O}$  nuclei followed by proton or neutron emission, and subsequent gamma decay of excited  $^{15}\text{N}$  or  $^{15}\text{O}$  nuclei, as suggested in Ref. [16]. We describe this signal and its time structure in Section II. In Section III we discuss the most relevant case of small masses. We find the smallest  $\nu_x$  mass that is recognizably different from zero in the presence of the expected finite counting statistics. In Section IV we show that the mass range is also limited from above. If the  $\nu_x$  mass is too large, the signal is broadened to such a degree that it disappears into the unavoidable background. We find the largest detectable  $\nu_x$  mass. Finally, in Section V we summarize our findings.

## II. CHARACTERISTICS OF THE MODEL

### A. Neutrino scattering rate

We assume that the double differential number distribution of neutrinos of a given flavor (one of  $\nu_e, \bar{\nu}_e, \nu_\mu, \bar{\nu}_\mu, \nu_\tau, \bar{\nu}_\tau$ ) at the source can be written in the product form:

$$\frac{d^2 N_\nu}{dE dt_i} = F(E) G(t_i), \quad (3)$$

where  $E$  is the neutrino energy and  $t_i$  is the time at the source. The double integral of this quantity is the total number of emitted neutrinos of that flavor  $N_\nu$ . This form assumes that the energy spectrum  $F(E)$  is time-independent; the time dependence of the source is parametrized solely by  $G(t_i)$ . The reasons for assuming that the energy and time dependences are separable will be given below. The most general form would allow  $F = F(E, t_i)$ , e.g., a time-dependent temperature. The luminosity is

$$L(t_i) = \int dE E \frac{d^2 N_\nu}{dE dt_i} = \langle E \rangle G(t_i) \int dE F(E), \quad (4)$$

where  $\langle E \rangle$  is the (time-independent) average energy. If the energy spectrum is normalized as

$$f(E) = \frac{F(E)}{\int dE F(E)}, \quad (5)$$

then we can write

$$\frac{d^2 N_\nu}{dE dt_i} = f(E) \frac{L(t_i)}{\langle E \rangle}. \quad (6)$$

This form is convenient since we assume, as stated earlier, that the luminosities of the different flavors are approximately equal at every time  $t_i$ . The energy spectrum  $f(E)$  will be taken to be thermal, and the luminosity  $L(t_i)$  will be taken to have a very sharp rise and an exponential decline. The arrival time of a neutrino of mass  $m$  at the detector is  $t = t_i + D + \Delta t(E)$ , where  $D$  is the distance to the source, and the energy-dependent time delay is given by Eq. (2). For convenience, we drop the constant  $D$ . Then the double differential number distribution of neutrinos at the detector is given by

$$\begin{aligned} \frac{d^2 N_\nu}{dE dt} &= \int dt_i \frac{d^2 N_\nu}{dE dt_i} \delta(t - t_i - \Delta t(E)) \\ &= f(E) \frac{L(t - \Delta t(E))}{\langle E \rangle}. \end{aligned} \quad (7)$$

Note that because of the mass effects, this is no longer the product of a function of energy alone and a function of time alone. The number flux of neutrinos at the detector is obtained by dividing this by  $4\pi D^2$ . The scattering rate for a given neutrino reaction is then

$$\frac{dN_{sc}}{dt} = N_{H_2O} n \int dE \sigma(E) \frac{1}{4\pi D^2} \frac{d^2 N_\nu}{dE dt}, \quad (8)$$

where  $N_{H_2O}$  is the number of water molecules in the detector,  $\sigma(E)$  the cross section for a neutrino of energy  $E$  on the target particle, and  $n$  the number of targets per water molecule for the given reaction. Using the results above,

$$\frac{dN_{sc}}{dt} = N_{H_2O} \frac{1}{4\pi D^2} \frac{1}{\langle E \rangle} n \int dE \sigma(E) f(E) L(t - \Delta t(E)). \quad (9)$$

In more convenient units, the scattering rate (per s) is:

$$\frac{dN_{sc}}{dt} = C \int dE f(E) \left[ \frac{\sigma(E)}{10^{-42} \text{cm}^2} \right] \left[ \frac{L(t - \Delta t(E))}{E_B/6} \right], \quad (10)$$

where

$$C = 9.21 \left[ \frac{E_B}{10^{53} \text{ ergs}} \right] \left[ \frac{1 \text{ MeV}}{T} \right] \left[ \frac{10 \text{ kpc}}{D} \right]^2 \left[ \frac{\text{det. mass}}{1 \text{ kton}} \right] n, \quad (11)$$

$T$  is the spectrum temperature (where we assume  $\langle E \rangle = 3.15T$ , as appropriate for a Fermi-Dirac spectrum), and  $f(E)$  is in  $\text{MeV}^{-1}$ . Since the luminosities are equal for each flavor, the total binding energy released in a given flavor is  $E_B/6$  (we ignore the small effect associated with the neutronization burst). When an integral over all arrival times is made, the luminosity term in square brackets integrates to one, giving for the total number of scattering events:

$$N_{sc} = C \int dE f(E) \left[ \frac{\sigma(E)}{10^{-42} \text{cm}^2} \right]. \quad (12)$$

The formulae in this section were derived for a nonzero neutrino mass; for massless neutrinos, simply take  $\Delta t(E) = 0$  throughout. In particular, note that in Eq. (10) the luminosity term then can be taken outside of the integral, making the time dependence of the scattering rate simply a constant times the time dependence of the luminosity.

## B. Details of the model

As noted above, we assume that the energy distribution for a given flavor of neutrinos is time-independent, e.g., that the temperature does not vary with time. While the temperature really will vary with time, the variation is probably not large (see e.g., Fig. 3 of Ref. [2], but note that those “average” energies are defined as  $\langle E^2 \rangle / \langle E \rangle$ ). Also, recent numerical models of supernovae disagree on the form of the variation, and even whether it is rising or falling. A well-motivated form for temperature variation may eventually be obtained from the supernova  $\bar{\nu}_e$  data or from more-developed numerical models. The analysis of this paper could be easily modified to allow a varying temperature; until there is a compelling reason to use a particular form, we simply use a constant temperature.

The energy distribution is taken to be a Fermi-Dirac distribution, characterized only by a temperature. We take  $T = 8$  MeV for  $\nu_x$ ,  $T = 5$  MeV for  $\bar{\nu}_e$ , and  $T = 3.5$  MeV for  $\nu_e$ . These temperatures are consistent with numerical models, e.g., in Ref. [3]. More elaborate models also introduce a chemical potential parameter to reduce the high-energy tail of the Fermi-Dirac distribution. That reduces the number of scattering events, but makes the dominant contribution to the cross section occur at a lower neutrino energy, thus giving a larger delay.

Numerical supernova models suggest that the neutrino luminosity rises quickly over a time of order 0.1 s, and then falls over a time of order several seconds. Therefore, the luminosity used in our numerical simulation is composed of two pieces. The first gives a very short rise from zero to the full height over a time 0.09 s, using one side of a Gaussian with  $\sigma = 0.03$  s. The rise is so fast that the details of its shape are irrelevant. The second piece is an exponential decay with time constant  $\tau = 3$  s. The luminosity then has a width of 10 s or so, consistent with the SN 1987A observations. The detailed form of the neutrino luminosity is less important than the general shape features and their characteristic durations. In Ref. [2], the neutrino luminosity actually decreases as a power law, and does so somewhat faster than our exponential. The slower the decay, the harder it is to see mass effects, so our choice is actually somewhat conservative.

Throughout the paper, we assume that the distance to the supernova is  $D = 10$  kpc, approximately the distance to the Galactic center.

## C. Characteristics of SuperKamiokande

In this paper, all of the results are for the SuperKamiokande (SK) detector. The analysis here could be easily applied to any water-Cherenkov detector. Its large size, low threshold, and low background rate make it very well-suited to detect a Galactic supernova. We assume an energy threshold of 5 MeV; presently it is a little bit higher but has been lowered a few times. The full volume of the main tank is 32 kton. From SK conference talks [17], we estimate the time-independent background rate for the inner fiducial 22.5 kton volume to be about  $0.1 \text{ s}^{-1}$  for a threshold of 5 MeV. For the full 32 kton volume, we estimate that the background rate can be no more than several times worse than  $0.1 \text{ s}^{-1}$ , again for a threshold of 5 MeV. For the low-mass search in Section III, we assume that the full 32 kton volume is used. The exact value of the time-independent background rate is completely irrelevant in that search. For the high-mass search in Section IV, we assume that only the inner 22.5 kton will be used, since in that case the time-independent background rate would be an important factor. Using only the inner volume will decrease the number of signal events by a factor 1.4, while decreasing the background by a factor of at least a few.

## D. Description of the signal

The cross section for the neutral-current excitation of  $^{16}\text{O}$  by neutrinos was computed numerically in Ref. [16]. It was assumed to be a two-step process, of excitation of  $^{16}\text{O}$  to the continuum, followed by decays into various final states. The principal branches in this decay are to states of  $^{15}\text{N} + \text{p}$  and  $^{15}\text{O} + \text{n}$ . For  $\nu_x$  neutrinos with a thermal spectrum with  $T = 8$  MeV, the combined branching ratio for these final states is about 95%. If the decay is to a bound excited state of the daughter nucleus, then the daughter will decay by gamma emission. At the relevant excitation energies in  $^{16}\text{O}$ , the branching ratio to these states in the daughters is about 30%. The crucial point is that in both  $^{15}\text{N}$  and  $^{15}\text{O}$  all gamma rays lie between 5 and 10 MeV and can thus be detected in SK. The other 70% of the branching ratio involves decays to the ground state of the daughters without gamma emission. In order to get to a final state with a gamma, the neutrino energy must be greater than about 20 MeV. Because of this high threshold, and because of the lower  $\nu_e$  and  $\bar{\nu}_e$  temperatures, these reactions contribute only at the 2% level compared to the  $\nu_x$  reactions, and hence are ignored [16].

In Refs. [16,18], the neutral-current cross sections were calculated numerically and folded with thermal neutrino spectra of different temperatures. For the present purpose we need the cross section for a given neutrino energy. It turns out that the simple parameterized form  $\sigma(E) = \sigma_0(E - 15)^4$ , with the neutrino energy  $E$  in MeV

and  $\sigma_0 = 0.75 \times 10^{-47} \text{ cm}^2$  describes quite well the cross section for a neutrino to excite  $^{16}\text{O}$ . In the fit we assumed that the branching ratio for states that end with gamma emission is independent of neutrino energy. All such branches are included in this cross section above, and we have summed the cross sections for neutrinos and antineutrinos (for just one flavor), as well as both final channels. The fit values agree with the numerical calculations at the 10% level over four orders of magnitude in the thermally-averaged excitation cross section. This fit will certainly not hold at higher energies which are however irrelevant in the present context.

In order to estimate the delay, Eq. (2) can be evaluated with a typical neutrino energy. However, one should not use the average energy,  $\langle E \rangle = 25 \text{ MeV}$ . Rather, one should use the energy for which  $f(E)\sigma(E)$  peaks. For this reaction, this ‘‘Gamow peak’’ energy is  $E \approx 60 \text{ MeV}$ , i.e., considerably larger than  $\langle E \rangle$ . The fact that the neutrinos have a spectrum of energies means that different values of  $E$  contribute to the time delay, causing dispersion of the neutrino pulse as it travels from the supernova. It turns out that for the small masses we are primarily interested in these dispersive effects are minimal.

The signal associated with the gamma emission described above will not be the dominant signal of a Galactic supernova in SuperKamiokande. Rather, the dominant events will be the positrons from  $\bar{\nu}_e + p \rightarrow e^+ + n$ , which give a smooth continuum in positron energy, peaking at about 20 MeV. The expected numbers of events for various reactions were calculated with Eq. (12) and are given in Table I. For the  $\bar{\nu}_e$  absorption on proton reaction, recoil and weak magnetism effects were taken into account, which slightly reduces the cross section. There are also charged-current reactions on  $^{16}\text{O}$  [19]; these increase the dominant positron signal by about 1%. Since events from the electron-scattering channels are forward-peaked, we assume that they are removed by an angular cut. Therefore, in our analysis we use only the events from  $\bar{\nu}_e$  absorption on protons and the  $\nu_x$  excitation of  $^{16}\text{O}$ .

The gammas from the neutral-current reactions above are at several discrete energies ranging from 5.2 MeV to 9.9 MeV. These are subject to some smearing, due to the finite resolution, giving few narrow peaks on top of the smooth distribution of positrons as shown in Fig. 2 of Ref. [16]. For simplicity, we treat the energy range from threshold to 10 MeV as one bin, and assume that losses due to the threshold or efficiency are minimal.

In Ref. [16] numbers of events from different reactions were calculated relative to each other, with the overall scale set by the total number of  $\bar{\nu}_e$  events from Ref. [20]. However, the number of  $\bar{\nu}_e$  events corresponding to  $T = 3 \text{ MeV}$  from Ref. [20] was used. This was not really consistent, and would not be consistent here either, since for the  $\bar{\nu}_e$  neutrinos,  $T = 5 \text{ MeV}$  is assumed here and in Ref. [16]. Consequently, we use instead Eq. (12) to calculate the number of events for  $T = 5 \text{ MeV}$ . We verified that the rates based on Eq. (12) agree with the numbers

TABLE I. Calculated numbers of events expected in SK with a 5 MeV threshold and a supernova at 10 kpc. The other parameters (e.g., neutrino spectrum temperatures) are given in the text. In rows with two reactions listed, the number of events is the total for both. The second row is a subset of the first row that is an irreducible background to the reactions in the third and fourth rows.

| reaction  | number of events |
|---|------------------|
| $\bar{\nu}_e + p \rightarrow e^+ + n$                                     | 8300             |
| $\bar{\nu}_e + p \rightarrow e^+ + n \quad (E_{e^+} \leq 10 \text{ MeV})$ | 530              |
| $\nu_\mu + ^{16}\text{O} \rightarrow \nu_\mu + \gamma + X$                | 355              |
| $\bar{\nu}_\mu + ^{16}\text{O} \rightarrow \bar{\nu}_\mu + \gamma + X$    |                  |
| $\nu_\tau + ^{16}\text{O} \rightarrow \nu_\tau + \gamma + X$              | 355              |
| $\bar{\nu}_\tau + ^{16}\text{O} \rightarrow \bar{\nu}_\tau + \gamma + X$  |                  |
| $\nu_e + e^- \rightarrow \nu_e + e^-$                                     | 200              |
| $\bar{\nu}_e + e^- \rightarrow \bar{\nu}_e + e^-$                         |                  |
| $\nu_\mu + e^- \rightarrow \nu_\mu + e^-$                                 | 60               |
| $\bar{\nu}_\mu + e^- \rightarrow \bar{\nu}_\mu + e^-$                     |                  |
| $\nu_\tau + e^- \rightarrow \nu_\tau + e^-$                               | 60               |
| $\bar{\nu}_\tau + e^- \rightarrow \bar{\nu}_\tau + e^-$                   |                  |

given in Ref. [20] when consistent temperatures are used. Note that the results of Ref. [16] are changed only by increasing the number of events in each reaction by a factor of about 2.

### III. LOW-MASS CASE

In this section, we detail the strategy used in the analysis. First, the  $\bar{\nu}_e$  mass is low enough that it can be neglected. Our final result is that one can reach sensitivity down to a  $\nu_x$  mass of about 50 eV. Since the  $\bar{\nu}_e$  mass is at least 10 times smaller, and since the delay depends quadratically on the mass, this neglect is justified. This establishes the key point of our technique: that we can use the  $\bar{\nu}_e$  events as a clock by which to measure the possible delay of the  $\nu_x$  neutrinos. Under our assumption that the temperatures are approximately constant, the only time dependence of the  $\bar{\nu}_e$  scattering rate is from the  $\bar{\nu}_e$  luminosity itself (see Eq. (10) with  $m = 0$ ). In contrast, the time dependence of the  $\nu_x$  scattering rate is determined both by the  $\nu_x$  luminosity and the delaying effects of a possible mass. Thus the effects of a mass can be tested for by comparing the scattering rates of the  $\bar{\nu}_e$  and  $\nu_x$  events as a function of time. In other words, we are looking for time dependence in the  $\nu_x$  rate beyond that expected from the luminosity variation alone. In order to implement this, we define two rates, as follows.

The scattering rate of  $\bar{\nu}_e$  events with  $E_{e^+} > 10 \text{ MeV}$  will be called the Reference  $R(t)$ . This contains  $\approx 8300 - 530 \approx 7800$  events. The time dependence of  $R(t)$  is completely determined by the time dependence of the luminosity. Its shape is generic for massless neutrinos. The Signal  $S(t)$  has three components. The first is the scattering rate for the 355 events from the com-

binned  $\nu_\mu$  and  $\bar{\nu}_\mu$  on  $^{16}\text{O}$  reactions. The second is the same for the 355 combined  $\nu_\tau$  and  $\bar{\nu}_\tau$  events. The third is the scattering rate for the 530  $\bar{\nu}_e$  events with  $E_{e^+} < 10$  MeV. We will assume that some portion of the Signal  $S(t)$  events are massive (either all  $\nu_\tau$  events or all  $\nu_\mu$  and  $\nu_\tau$  events). All of the other events in  $S(t)$  are then massless background events. Because some of the  $S(t)$  events will be massive, the shape of  $S(t)$  will be distorted. In particular, it will be delayed and broadened.

In a given experiment (i.e., one supernova), the Signal  $S(t)$  and the Reference  $R(t)$  will be measured. In order to facilitate comparison of their shapes, the curve  $R(t)$  can be scaled down to the number of events in  $S(t)$ . The curve  $S(t)$  shows how the data look, with a possible unknown  $\nu_\tau$  mass, and the curve  $R(t)$  shows how they would look if all of the events were massless. The rates are shown in Fig. 1, which depicts  $S(t)$  under different assumptions about the  $\nu_\tau$  mass. The shape of  $R(t)$  is the same as that of  $S(t)$  when  $m_{\nu_\tau} = 0$ . The curve  $R(t)$  will be measured, and so will be there to compare the measured  $S(t)$  to. As the  $\nu_\tau$  mass is increased, the delayed  $\nu_\tau$  events separate from the massless events more and more. For  $m = 125$  eV, the scattering rate over the first 1 s or so is just that from the remaining massless events. The effect of a mass is to diminish the rate at early times and enhance it at late times (since the normalization is preserved, these are roughly equivalent statements).

In a real experiment, statistical fluctuations will mask the effect of a mass. The Reference  $R(t)$  contains approximately 7800 events, and thus has small relative fluctuations. The Signal  $S(t)$  contains approximately 1240 events, and therefore has larger relative fluctuations. Each of those curves is subject to fluctuations in the total number of events as well as fluctuations in any time interval. Consider for a moment the events in the first 1 s of Fig. 1. There are 336 events expected in the  $m_{\nu_\tau} = 0$  eV case, and 302 events expected in the  $m_{\nu_\tau} = 50$  eV case. As noted, the Reference has smaller fluctuations, so for now take the total 336 as exact. The counting error on the Signal in that interval will be of order  $\sqrt{302} \approx 17$ . If the number of events in this bin fluctuates up by about two sigma, then the number of events in the Signal over this interval would match the number expected for the massless case, and we would have to conclude that most probably the mass of the  $\nu_\tau$  is zero. In the analysis below, we use much more of the data, but the idea is the same: it is possible for one mass case to fake another through fluctuations. The degree to which this can occur depends primarily on the number of events expected in the Signal. We will restrict the range of fluctuations that we consider to be likely by choosing confidence levels.

To treat the expected fluctuations properly, we use a Monte Carlo technique to generate representative statistical instances of the theoretical forms for  $R(t)$  and  $S(t)$ . Each run represents one supernova as seen in SK. The total number of events expected in  $R(t)$  is known. In each particular run, this total is subject to Poisson fluctua-

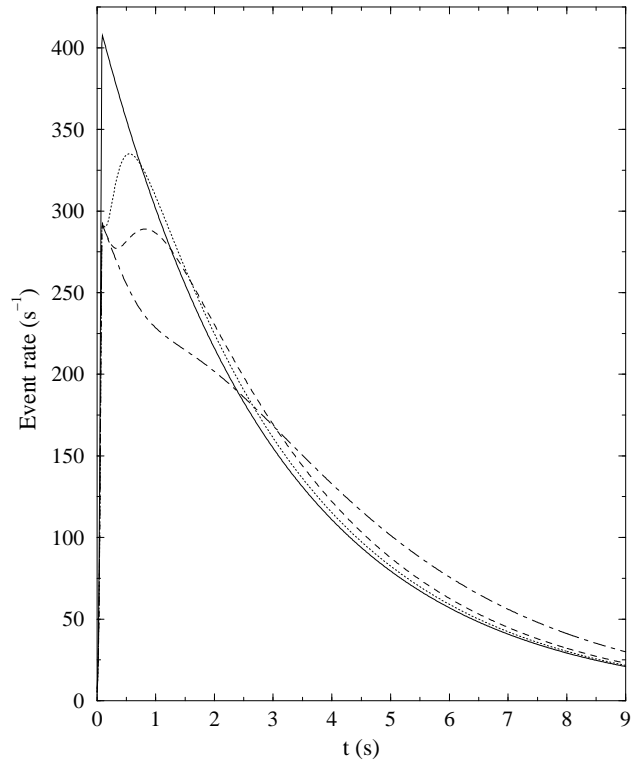


FIG. 1. The expected event rate in the absence of fluctuations for the signal  $S(t)$  is shown for different  $\nu_\tau$  masses, as follows: solid line, 0 eV; dotted line, 50 eV; dashed line, 75 eV; dot-dashed line, 125 eV. Of 1240 total events, 530 are massless  $\bar{\nu}_e$ , 355 are massless  $\nu_\mu$  and  $\bar{\nu}_\mu$ , and 355 are massive  $\nu_\tau$  and  $\bar{\nu}_\tau$ . These totals count events at all times; in the figure, only those with  $t \leq 9$  s are shown.

tions. We model this by picking a Poisson random number from a distribution with mean given by the expected number of events. This gives the number of events for this particular run. We then use an acceptance-rejection method to sample the form  $R(t)$  until the right number of events for that run is obtained. This gives a statistical instance of  $R(t)$ , typical of what might be seen in a single experiment. Then an exactly analogous technique is used to generate the total number of events in  $S(t)$  and a statistical instance of the curve  $S(t)$  itself. The massless and massive components of  $S(t)$  are sampled separately, and are then added together.

One comment on the method of sampling is necessary. No matter how the generated rates are binned in time, this method ensures that in each bin there are the correct Poisson fluctuations around the expected number in that bin. Therefore, this technique is equivalent to the sometimes-seen technique of first establishing bins and the expected number in each bin, and then picking a representative number of events for that bin according to the appropriate Poisson distribution. However, our method of generating representative Signal and Reference data sets does not require binning. If analysis of these data sets uses bins, the bin size can be changed without regenerating the data.

Both of the tests developed below depend upon the shape of  $S(t)$ , and not directly on the number of counts. Direct tests for an excess or deficit of counts are much more dependent on theory; this dependence is largely canceled in our approaches.

### A. $\chi^2$ analysis

As discussed above, the presence of a mass in the Signal  $S(t)$  will cause its relative decrease at early times and relative increase at late times in comparison with the Reference  $R(t)$ . Whether or not it can be seen is a question of the statistics of the event rates. As a first test we look for a shape distortion in  $S(t)$  relative to  $R(t)$  by making a  $\chi^2$  test. If the  $\chi^2$  per degree of freedom (d.o.f.) is of order unity, then the two curves are compatible at the level of the errors, and there is no reason to invoke a mass. If the  $\chi^2$ /d.o.f. is large, then the two functions are incompatible, which we take as evidence for a mass. That is, we assume that there are no other systematic effects which would give a large  $\chi^2$ /d.o.f.; one always has to make some such assumption.

We first scale the Reference down to the number of events observed in the Signal over the range  $0 \leq t \leq t_{max}$ . As required for a  $\chi^2$  test, both sets are then binned so the continuous functions  $R(t)$  and  $S(t)$  are replaced by discrete representations. Bins of constant width  $\delta t$  are used. The scaling is given by

$$\tilde{R}_j = R_j \frac{\sum_{j=1}^{N_{bin}} S_j \delta t}{\sum_{j=1}^{N_{bin}} R_j \delta t}, \quad (13)$$

where  $t_{max} = N_{bin} \delta t$ . When  $m = 0$ ,  $\tilde{R}_j = S_j$ , up to statistical fluctuations. The  $\chi^2$  is formed as follows:

$$\chi^2/\text{d.o.f.} = \frac{1}{N_{bin} - 1} \sum_{j=1}^{N_{bin}} \frac{(\tilde{R}_j \delta t - S_j \delta t)^2}{s \tilde{R}_j \delta t + S_j \delta t}, \quad (14)$$

where  $j$  runs over the bins used. The number of degrees of freedom is reduced by one because we have normalized the Reference to the Signal. The factor  $s$  is the ratio of the total numbers of events (in  $0 \leq t \leq t_{max}$ ) in the Signal and the Reference, and is computed for each run in the Monte Carlo. Even though  $\tilde{R}_j \delta t \approx S_j \delta t$ , the fluctuations in  $\tilde{R}_j \delta t$  are much smaller since  $\tilde{R}_j \delta t$  is scaled down from  $R_j \delta t$ , which has high statistics.

It is important to stress that it is not enough to evaluate the  $\chi^2$  using the predicted curves for  $R(t)$  and  $S(t)$  based on the analytic forms constructed with Eq. (10). Doing so neglects fluctuations, and always underestimates the  $\chi^2$ , particularly near the small-mass limit that we are interested in (since in the massless case  $\tilde{R}(t) = S(t)$ ). Roughly speaking, using the exact functions themselves in the  $\chi^2$  underestimates the  $\chi^2$ /d.o.f. by about unity, and of course does not give the error.

As explained above, we use the Monte Carlo technique which properly treats statistical fluctuations, and leads to a more conservative (and correct) mass limit.

Only a finite range of times was used in forming the  $\chi^2$ . The beginning of the first bin is taken to be where the events start. With some 9000 total events expected, and a risetime of order 0.1 s, the starting time can be reasonably well-defined. In the Monte Carlo, the starting time was held fixed (and not adjusted from the data on each run). The definition used amounts to calling the starting time that point at which the  $\bar{\nu}_e$  rate is about 1% of its peak rate. The size of any ambiguity in the starting time is much smaller than the bin size (discussed below), and so is regarded as irrelevant.

The ending time and the bin size must be chosen more carefully. The primary consideration is to maximize the extraction of the mass effect in the presence of the statistical fluctuations. Further, this must be optimized for the case of a small mass (other cases are discussed below). In Fig. 1, one can see that for a given  $m_{\nu\tau}$ , the Signal  $S(t)$  rejoins the Reference  $R(t)$  at very late times (even beyond the edge of the figure for the larger masses). Once this has happened, there is no benefit to going to larger times; in fact, one only includes more statistical noise by doing so. In the Monte Carlo studies, it was found that  $t_{max} = 9$  s and a bin size of  $\delta t = 1$  s were good choices (the final results are only weakly dependent on these). These are also very reasonable from a physical point of view. These have to be held fixed for all of the Monte Carlo runs, since one cannot adjust these to a particular data set without introducing bias. These choices also ensure that we can completely neglect the time-independent background rate of at most a few times  $0.1 \text{ s}^{-1}$ .

With these choices, one has a reasonable number (namely 8) of degrees of freedom in the  $\chi^2$ , and a large number of events expected in each bin. The latter ensures that the Poisson errors on the counts in each bin really are approximately Gaussian, as required in the  $\chi^2$  definition. Up to fluctuations, the late-time bins all have an excess. Combining them would enhance the significance of this excess, whereas for random fluctuations combining bins does not change the significance. The same is true for the early-time deficits. However, one does not in general know where the transition point is between these two regions; that is determined by the unknown mass. The transition point cannot be determined from the data without introducing bias. Also, with too few bins, one does not satisfy the requirements for defining a  $\chi^2$  test.

Using the above procedure for analyzing each run (and in particular, normalizing  $R(t)$  to  $S(t)$  over  $0 \leq t \leq t_{max}$ ), we used the Monte Carlo to simulate the results from  $10^4$  supernovae. For each run, the  $\chi^2$  analysis was performed. For each fixed mass, a variety of  $\chi^2$  values are obtained, due to the finite statistics in the Reference and the Signal. These results were histogrammed as  $\chi^2$ /d.o.f. The relative frequencies of different  $\chi^2$ /d.o.f. values are shown in the upper panel of Fig. 2 for a few represen-

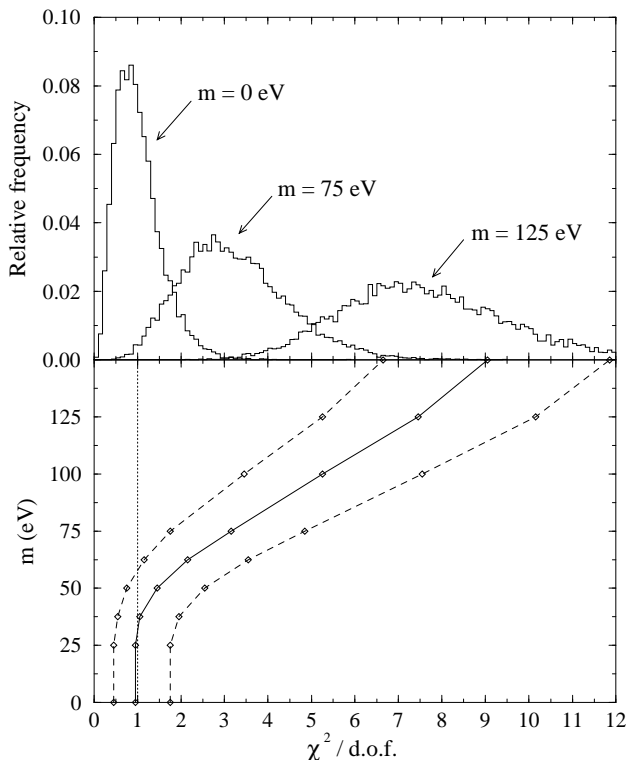


FIG. 2. The results of the  $\chi^2$  analysis for a massive  $\nu_\tau$ . In the upper panel, the relative frequencies of various  $\chi^2/\text{d.o.f.}$  values are shown for a few example masses. In the lower panel, the range of masses corresponding to a given  $\chi^2/\text{d.o.f.}$  is shown. The solid line is the 50% confidence level, and the upper and lower dashed lines are the 10% and 90% confidence levels, respectively. In this figure,  $t_{max} = 9$  s, the bin size used in the  $\chi^2$  is  $\delta t = 1$  s, and the time constant of the exponential luminosity is  $\tau = 3$  s.

tative masses. (Note that the number of Monte Carlo runs determines only how smoothly these distributions are filled out; their shape and placement is determined by the physics.) For  $m = 0$ , the resulting  $\chi^2/\text{d.o.f.}$  values of course fill out the usual  $\chi^2/\text{d.o.f.}$  distribution with 8 degrees of freedom.

These distributions are characterized by their central point and their (asymmetric) width, using the 10%, 50%, and 90% confidence levels. That is, for each mass we determined the value of  $\chi^2/\text{d.o.f.}$  such that a given percentage of the Monte Carlo runs yielded a value of  $\chi^2/\text{d.o.f.}$  less than that value. With those three numbers, we can characterize the results of complete runs with many masses much more compactly, as shown in the lower panel. For convenience, the axes are inverted from how the plot was actually constructed. That is, given the  $\chi^2/\text{d.o.f.}$  which will be experimentally determined, one can read off the range of masses that could have likely given such a  $\chi^2/\text{d.o.f.}$  at these confidence levels.

## B. $\langle t \rangle$ analysis

The  $\chi^2$  test above has the nice feature that it is a shape test, and depends on the number of events only through the fluctuations. One disadvantage is its dependence on binning, which obscures changes over timescales smaller than of order the bin width, i.e., the effects of sufficiently small masses. Another is that the mass effect is not always in the same sense. At early times there is a deficit of events, whereas at late times there is an excess; the  $\chi^2$  is insensitive to the difference between this distinctive feature and random fluctuations of similar magnitude. To get around these problems, we introduce here tests of integral moments. These do not involve any binning. The most basic effect of a mass is a delay; the average arrival time always increases. The test is simple, intuitively obvious, and the effect is always in the same sense (up to statistical fluctuations). A mathematically analogous moments analysis was made for electron recoil energies in the context of solar neutrino oscillations in Ref. [21].

Given the Reference  $R(t)$ , the average arrival time is defined as

$$\langle t \rangle_R = \frac{\sum_k t_k}{\sum_k 1} = \frac{\int_0^{t_{max}} dt t R(t)}{\int_0^{t_{max}} dt R(t)}. \quad (15)$$

The summation form is used for the Monte Carlo generated data sets, where the sum is over events (not time bins) in the Reference with  $0 \leq t \leq t_{max}$ . The integral form would be used if the theoretical forms for the rates were given. It is no longer necessary to normalize the Reference to the Signal. As with the  $\chi^2$  test, the starting time is assumed to be well-defined. The choice of  $t_{max}$  follows from similar considerations as before. The effect of the finite number of counts in  $R(t)$  is to give  $\langle t \rangle_R$  a statistical error. This error is the intrinsic width of the  $R(t)$  distribution divided by the square root of the number of events in the Reference. Both the intrinsic width and number of events depend on the choice of  $t_{max}$ . By choosing a moderate  $t_{max}$ , the intrinsic width of  $R(t)$  can be restricted even while most events are included.

Given the Signal  $S(t)$ , the average arrival time is defined similarly as

$$\langle t \rangle_S = \frac{\sum_k t_k}{\sum_k 1} = \frac{\int_0^{t_{max}} dt t S(t)}{\int_0^{t_{max}} dt S(t)}, \quad (16)$$

where naturally the sums are now over events in the Signal. While the intrinsic widths of  $R(t)$  and  $S(t)$  are similar, the statistical error on  $\langle t \rangle_S$  is larger by factor of a few since there are several times fewer events. The effect of the mass is to make  $\langle t \rangle_S$  larger, i.e., to cause a delay. (The mass increases the intrinsic width of  $S(t)$  only slightly.)

In order to cancel some systematic effects, we consider not  $\langle t \rangle_S$  as compared to theory but the difference  $\langle t \rangle_S - \langle t \rangle_R$  determined from the data. The signal of a mass is

that this is greater than zero with statistical significance. From the Monte Carlo studies,  $t_{max} = 9$  s was found to be a very reasonable choice; most of the data are then included while the range is kept small. For this  $t_{max}$ , the time-independent background events are negligible. Again, while these choices are somewhat optimal, the final results are not strongly dependent on the particular values used as long as they are reasonable. Although the values of  $\langle t \rangle$  depend on  $t_{max}$ , the dependence is not strong. For  $t_{max} = 9$  s, a change of 0.1 s in  $t_{max}$  gives a change of about 0.01 s in  $\langle t \rangle$ . Note that any shift in the starting time will cancel in the difference  $\langle t \rangle_S - \langle t \rangle_R$  (as long as it doesn't change the numbers of events included).

Using the above procedure for analyzing a particular run, we again used the Monte Carlo to simulate the results from  $10^4$  supernovae. Basically, things were done as above for  $\chi^2$ . For each run,  $\langle t \rangle_S - \langle t \rangle_R$  was calculated and its value histogrammed. These distributions are again characterized by their central point and their width, using the 10%, 50% (now also the average), and 90% confidence levels. That is, for each mass we determined the values of  $\langle t \rangle_S - \langle t \rangle_R$  such that a given percentage of the Monte Carlo runs yielded a value of  $\langle t \rangle_S - \langle t \rangle_R$  less than that value. Since these distributions are Gaussians, other confidence levels can easily be constructed. The results of this analysis are shown in Fig. 3, which is analogous to Fig. 2.

For  $t_{max} = 9$  s,  $\langle t \rangle_R = 2.57$  s. For larger  $t_{max}$ ,  $\langle t \rangle_R$  tends to about 3 s, the value of the exponential time constant in the luminosity. The value of  $\langle t \rangle_S$  is of course larger by the mass effect. As noted, the error on each moment is the intrinsic width divided by the square root of the number of events. The intrinsic widths of the  $R(t)$  and  $S(t)$  distributions are each of order a few seconds. The numbers of events are of order 8000 and 1200, respectively. Note that the errors on  $\langle t \rangle_R$  and  $\langle t \rangle_S$  are uncorrelated.

We also investigated the dispersion of the event rate in time as a measure of the mass. As noted above, a mass alone causes a delay, but a mass and an energy spectrum also cause dispersion. We defined the dispersion as  $\sqrt{\langle t^2 \rangle - \langle t \rangle^2}$ , where all integrals are as above defined up to  $t_{max}$ . We found that the effects were not statistically significant until the mass was of order 150 eV or so; at such a large mass the statistical significance of the change in  $\langle t \rangle$  cannot be missed.

### C. Comparison of techniques

The analysis techniques presented above are appropriate for the case in which the mass is either small or zero. In this case, the signal  $S(t)$  and the reference  $R(t)$  are not easily distinguished for finite statistics. Both the  $\chi^2$  and  $\langle t \rangle$  analyses were optimized for this case by choosing a moderate  $t_{max} = 9$  s, which also allowed us to neglect the time-independent background. In each case, sensitivity

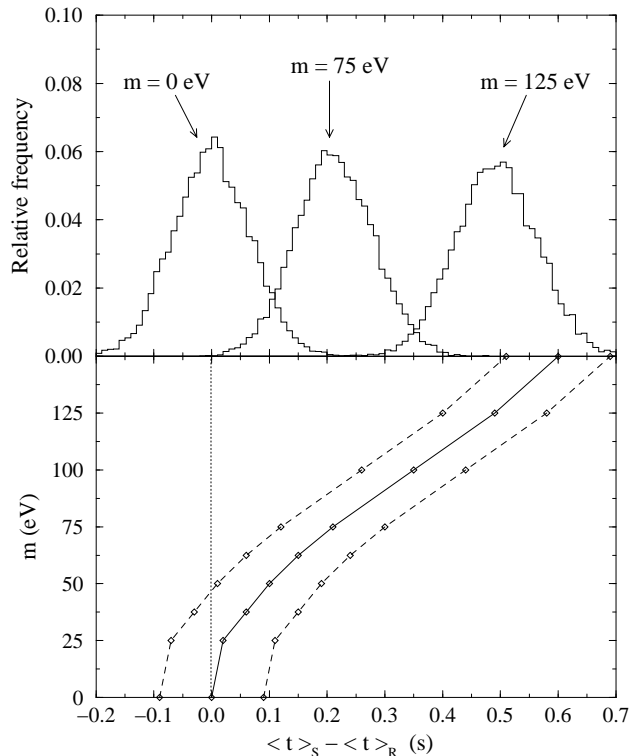


FIG. 3. The results of the  $\langle t \rangle$  analysis for a massive  $\nu_\tau$ . In the upper panel, the relative frequencies of various  $\langle t \rangle_S - \langle t \rangle_R$  values are shown for a few example masses. In the lower panel, the range of masses corresponding to a given  $\langle t \rangle_S - \langle t \rangle_R$  is shown. The solid line is the 50% confidence level, and the upper and lower dashed lines are the 10% and 90% confidence levels, respectively. In this figure,  $t_{max} = 9$  s and the time constant of the exponential luminosity is  $\tau = 3$  s.

to a  $\nu_\tau$  mass of about 50 eV was found. This is essentially the mass which cannot be missed even if there are unfavorable statistical fluctuations. Since the mass effects grow quadratically, for larger masses the statistical significance of the mass effects would be huge.

At a given mass, the ranges of  $\chi^2$  or  $\langle t \rangle_S - \langle t \rangle_R$  values shown in the figures are the ranges of probable values that would be seen in one experiment (i.e., one supernova). Those ranges are the result of properly taking into account the expected statistical fluctuations of the Reference and Signal (while the Signal error dominates, the Reference error was included in the calculations). For a given experiment, the values of  $\chi^2$  and  $\langle t \rangle_S - \langle t \rangle_R$  can be computed from the data. The statistical errors on those quantities can also be estimated from the data, and should be similar to what is shown in the figures.

The results from both analysis techniques are essentially similar. That is, the final results are not strongly dependent on the statistical technique used, which is crucial. Of course, the results from the  $\langle t \rangle$  analysis are slightly better, for the reasons explained above. The final figures for the  $\langle t \rangle$  analysis also allow other confidence levels to be constructed easily. Our  $\chi^2$  test was designed



TABLE II. The results of the  $\chi^2$  analysis for different cases. The decay constant of the exponential luminosity is denoted by  $\tau$ . If the masses are zero, the most probable  $\chi^2/\text{d.o.f.} = 1$ . For this  $\chi^2/\text{d.o.f.}$ , the allowed mass ranges are given in the second column; the lower limit of zero is the most probable mass, and the upper limit is excluded at the 90% confidence level. The smallest value of  $\chi^2/\text{d.o.f.}$  not compatible with  $m = 0$  is  $\chi^2/\text{d.o.f.} = 1.7$ . The corresponding allowed mass ranges are given in the third column; both the upper and lower limits are excluded at the 90% confidence level. The most probable mass is given in parentheses.

| case  | result for $\chi^2/\text{d.o.f.} = 1$ | result for $\chi^2/\text{d.o.f.} = 1.7$              |
|---|---------------------------------------|--|
| $\tau = 3\text{s}; m_{\nu_\mu} = 0, m_{\nu_\tau} = m$ | $0 \leq m < 60 \text{ eV}$            | $0 < m < 75 \text{ eV}$ ( $m \simeq 55 \text{ eV}$ ) |
| $\tau = 3\text{s}; m_{\nu_\mu} = m_{\nu_\tau} = m$    | $0 \leq m < 40 \text{ eV}$            | $0 < m < 50 \text{ eV}$ ( $m \simeq 40 \text{ eV}$ ) |
| $\tau = 1\text{s}; m_{\nu_\mu} = 0, m_{\nu_\tau} = m$ | $0 \leq m < 35 \text{ eV}$            | $0 < m < 45 \text{ eV}$ ( $m \simeq 30 \text{ eV}$ ) |

TABLE III. The results of the  $\langle t \rangle$  analysis for different cases. The decay constant of the exponential luminosity is denoted by  $\tau$ . If the masses are zero, the most probable  $\langle t \rangle_S - \langle t \rangle_R = 0$ . For this  $\langle t \rangle_S - \langle t \rangle_R$ , the allowed mass ranges are given in the second column; the lower limit of zero is the most probable mass, and the upper limit is excluded at the 90% confidence level. The smallest value of  $\langle t \rangle_S - \langle t \rangle_R$  not compatible with  $m = 0$  is  $\langle t \rangle_S - \langle t \rangle_R = 0.09 \text{ s}$ . The corresponding allowed mass ranges are given in the third column; both the upper and lower limits are excluded at the 90% confidence level. The most probable mass is given in parentheses. For the third case, because of the reduced width of the pulse, 0.03 s is used instead of 0.09 s.

| case  | result for $\langle t \rangle_S - \langle t \rangle_R = 0$ | result for $\langle t \rangle_S - \langle t \rangle_R = 0.09 \text{ s}$ |
|---|--|---|
| $\tau = 3\text{s}; m_{\nu_\mu} = 0, m_{\nu_\tau} = m$ | $0 \leq m < 45 \text{ eV}$                                 | $0 < m < 70 \text{ eV}$ ( $m \simeq 45 \text{ eV}$ )                    |
| $\tau = 3\text{s}; m_{\nu_\mu} = m_{\nu_\tau} = m$    | $0 \leq m < 35 \text{ eV}$                                 | $0 < m < 45 \text{ eV}$ ( $m \simeq 35 \text{ eV}$ )                    |
| $\tau = 1\text{s}; m_{\nu_\mu} = 0, m_{\nu_\tau} = m$ | $0 \leq m < 25 \text{ eV}$                                 | $0 < m < 40 \text{ eV}$ ( $m \simeq 25 \text{ eV}$ )                    |

to ask if there was evidence for a nonzero mass, the evidence being a large  $\chi^2$ . Strictly speaking, if there was such evidence the mass would not be determined with that test; one would reformulate the Reference to include a mass and would define a new  $\chi^2$ , which would be minimized with respect to the mass. Nevertheless, our formulation works reasonably for small masses. Finally, because of its greater convenience in use and interpretation, as well as its greater sensitivity, we advocate the  $\langle t \rangle$  technique.

We also considered the case in which both the  $\nu_\mu$  and the  $\nu_\tau$  are massive. For convenience, we took  $m_{\nu_\mu} = m_{\nu_\tau}$ . (Since the time delay is quadratic in the mass, there is little difference from the one-mass case unless the masses are similar.) The results of the  $\chi^2$  analysis are shown in Fig. 4, and the results of the  $\langle t \rangle$  analysis are shown in Fig. 5. As expected, with a better proportion of massive events in the Signal, lower masses can be probed. All of the results are summarized in Tables II and III.

#### D. Comparison to previous work

Various techniques for determining or limiting the  $\nu_\mu$  and  $\nu_\tau$  masses from observations of supernova neutrinos have been proposed. Any such technique must be based on a neutral-current signal and by necessity will contain events from other reactions with similar signatures but caused by  $\nu_e$  or  $\bar{\nu}_e$ . Also, in neutral current events, one cannot determine the initial neutrino energy on the event by event basis. (In the neutrino-electron scattering that is possible in principle, but not in practice). Hence, one

cannot directly determine the energy spectra of the incoming  $\nu_x$  neutrinos.

The most developed technique uses the signal from neutrino-electron scattering in SK. All flavors participate in this reaction, which has no threshold. Even though the  $\nu_\mu$  and  $\nu_\tau$  energies are higher, their thermally-averaged cross sections are smaller than for  $\nu_e$  and  $\bar{\nu}_e$  (which also have a charged-current channel). Thus massless events are necessarily part of the irreducible background. There are also isotropic background events from the copious  $\bar{\nu}_e + p \rightarrow e^+ + n$  reaction; by considering only events in the forward cone of half-angle about 25 degrees (determined by the angular resolution of the Čerenkov detector), one can eliminate about 95% of the isotropic background [10,12]. From Table I it follows that if just the  $\nu_\tau$  is massive, in the forward cone there are about 700  $m = 0$  events and about 60  $m > 0$  events. The test for a mass is to check whether the events in the forward cone fall off more slowly in time than those outside the cone. Since the number of massive events is small, one has to look for a large delay. At such late times in the tails of the scattering rates, the time-independent background rate is not at all negligible.

The most detailed analysis of the neutrino-electron scattering case was given in Ref. [10]. The statistical test for a mass was done by a complicated likelihood matching scheme, and sensitivity to a mass of about 50 eV was found. Another detailed analysis was given in Ref. [12]. The statistical test for a mass was simple, and was based on looking for an excess of events at late times, where an excess was defined as three times the Poisson error. In this case, sensitivity to a mass of only about 150 eV was found. The question arises if this poorer limit was

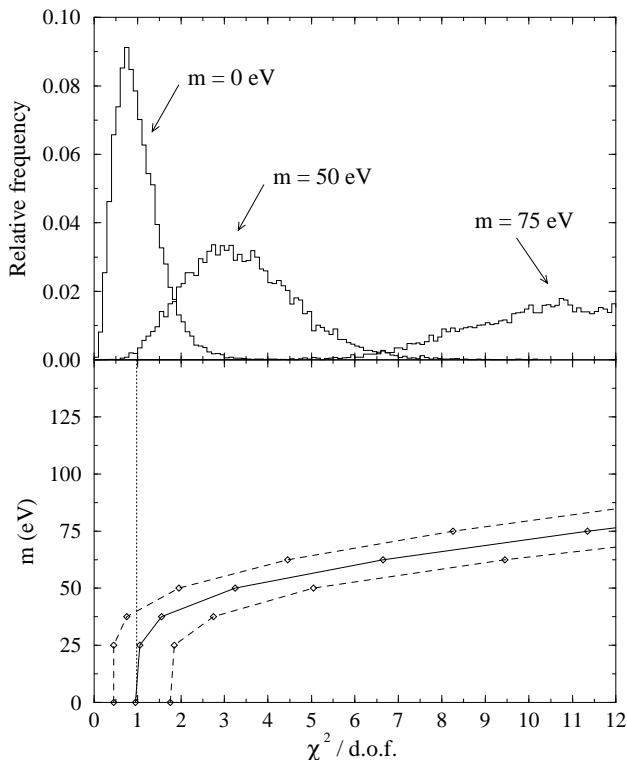


FIG. 4. The results of the  $\chi^2$  analysis for a massive  $\nu_\mu$  and  $\nu_\tau$ , taken to have the same mass. The figure is otherwise the same as Fig. 2.

caused by the less sophisticated statistical technique. Interestingly, it is not. It is pointed out in Ref [12] that the authors of Ref. [10] use a luminosity which decays roughly exponentially, with a time constant of  $\tau = 1$  s (in contrast to the time constant of  $\tau = 3$  s used in this work). Such a sharp time distribution makes distinguishing the effects of a mass much easier. In Ref. [12], it is shown that using such a quickly-decaying luminosity and the same simple statistical technique that sensitivity to 50 eV can also be obtained.

For comparison, we set the exponential time constant in the luminosity to  $\tau = 1$  s and repeated our analysis. For  $t_{max} = 3$  s and a bin size of 0.5 s, we found sensitivity to about 25 eV in the one-mass case. The results are also presented in Tables II and III. The advantages of the method discussed here, as demonstrated by this comparison, are the larger number of events with mass and the lower proportion of massless events with a similar signature.

#### IV. INTERMEDIATE-MASS AND HIGH-MASS CASES

For a low or zero mass ( $m_{\nu_\tau} \lesssim 150$  eV), the effects on the signal  $S(t)$  are minimal, and the time-independent background is negligible. For an intermediate mass ( $150 \text{ eV} \lesssim m_{\nu_\tau} \lesssim 1 \text{ keV}$ ), the effects on  $S(t)$  are sub-

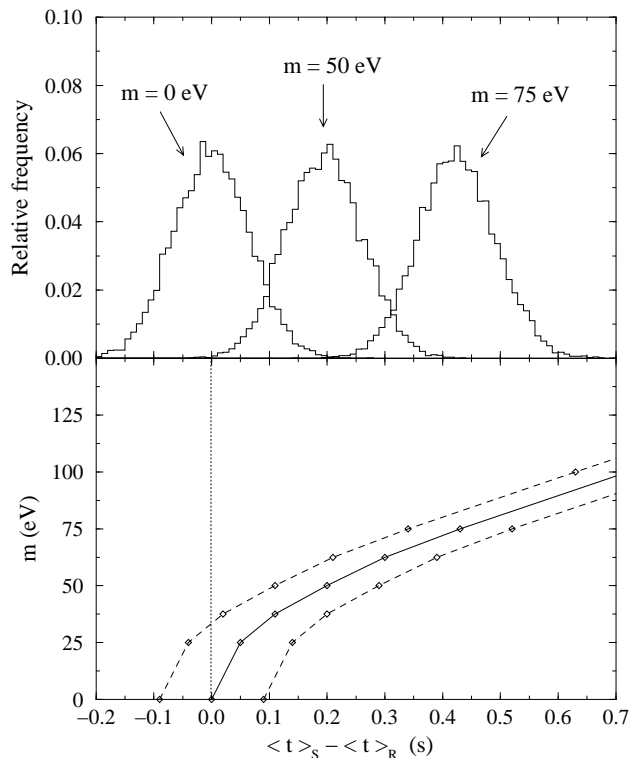


FIG. 5. The results of the  $\langle t \rangle$  analysis for a massive  $\nu_\mu$  and  $\nu_\tau$ , taken to have the same mass. The figure is otherwise the same as Fig. 3.

stantial, and the massive component of  $S(t)$  will be well-separated from the the massless component. The time-independent background does not have a large effect, but would have to be taken into account. For a large mass ( $m_{\nu_\tau} \gtrsim 1 \text{ keV}$ ), the massive component of  $S(t)$  is so delayed and dispersed that its rate is comparable to or below the time-independent background rate. Given the actual data, one can immediately determine which of these cases applies. There are analysis techniques that are optimal for each case. It is “fair” to determine the choice of technique from the crude characteristics of the data.

The intermediate-mass case would be rather easy to handle. The value of  $t_{max}$  would have to be increased and the time-independent background rate included. The  $\chi^2$  analysis above was designed to test whether or not a mass was necessary to explain the data. For a small mass, it can be used to determine that mass. As noted earlier, for a large and obvious mass, it would be better to revise the  $\chi^2$  analysis so that the Reference  $R(t)$  was that appropriate for a given mass. Then the  $\chi^2$  could be minimized to find the unknown mass and its error. The  $\langle t \rangle$  technique requires only the changes noted. For such a large mass, the dispersion (broadening) also becomes a useful measure of the mass. Almost any technique would work in this case since the signal will be so obvious.

The large-mass case, like the low-mass case, is again a marginal analysis since we are by definition looking at the limit of detectability. For a large mass, the delays are

large compared to the width of the pulse at the source, and the integral in Eq. (10) can be evaluated by assuming that the time distribution of the initial pulse is a delta function. The scattering rate (per s) is

$$\frac{dN_{sc}}{dt} = \frac{C}{2t} \tilde{E} f(\tilde{E}) \left[ \frac{\sigma(\tilde{E})}{10^{-42} \text{cm}^2} \right], \quad (17)$$

where  $C$  is defined in Eq. (11), and  $\tilde{E}$  in MeV is defined as  $\tilde{E} = m\sqrt{0.515D/t}$  (see Eq. (2)), with  $m$  in eV,  $D$  in 10 kpc, and  $t$  in s. Note also that  $f$  is in  $\text{MeV}^{-1}$ . The time  $t$  is measured from the arrival of the  $\bar{\nu}_e$  events. For  $m = 1$  keV, the signal is still several times the time-independent background for hundreds of seconds. As the mass increases, the height of the signal rate falls very quickly.

Even if  $S(t) < B$  at all times, where  $B$  is the time-independent background rate, it is still possible to determine a mass by looking for an excess of counts in some long time interval. We assume that the expected number of signal events is present (the Poisson fluctuation of the signal number will turn out to be a small effect). This analysis is therefore more model-dependent than the low-mass case, since the number of events enters directly, rather than only through the fluctuations. While  $t$  is defined by the arrival of the  $\bar{\nu}_e$  events, they are obviously not included in the counts for this analysis. Only a finite range of neutrino energies contribute significantly, and the largest energy is of order 5 times the smallest. The largest delay will thus be of order 25 times the smallest. In this case, the simplest and most model-independent thing to do is to begin the counting at  $t = 0$ .

We assume that the background rate  $B$  is well-known. The end of the counting interval  $t_{max}$  is to be determined. The requirement of a statistically significant excess of counts is  $N_B + N_S > N_B + n\sqrt{N_B}$ , where  $n$  is the number of sigmas (the number of counts is large enough to treat the Poisson distribution as a Gaussian.) Any large excess in the number of events will be wholly attributed to the signal events, of which there are  $N_S$  expected. Using  $N_B = Bt_{max}$ , this can be rewritten as  $t_{max} < N_S^2/n^2B$ . Note that this is independent of mass. The requirements for  $t_{max}$  are:

$$\text{signal width} < t_{max} < \frac{N_S^2}{n^2B}. \quad (18)$$

If the interval is not as wide as the signal, signal events will be lost. If it is wider than the signal, too many background events will be included. The largest possible mass that can be seen with this technique is the one for which the signal width is as wide as the right-hand side of the equation above. This is

$$m_{max} = E_{min} \frac{N_S}{n\sqrt{0.515DB}}, \quad (19)$$

where  $m$  is in eV,  $E_{min}$  is in MeV,  $D$  is in 10 kpc, and  $B$  is in  $\text{s}^{-1}$ . For the  $\nu_x$  excitation of  $^{16}\text{O}$ , we take  $E_{min} = 25$

MeV; below that energy, the product  $f(E)\sigma(E)$  is essentially zero. In order to reduce the time-independent background rate, we use only the inner 22.5 kton volume for this large-mass test, which reduces the number of  $\nu_\tau$  signal events to  $N_S = 250$ . For this volume, the background rate has been measured [17] to be of order  $0.1 \text{ s}^{-1}$ . At the three-sigma level ( $n = 3$ ), the maximum detectable mass is then about  $m_{max} = 9$  keV. For this mass, even the peak of the signal rate is a factor several below the time-independent background rate. Also for this mass,  $t_{max}$  is of order  $10^5$  s, so the Poisson error on the number of background events is at the 1% level. We have assumed that the error on the background rate  $B$  is not larger than that. The above analysis is optimized for a flat signal. However, the signal is actually peaked at a time smaller than  $t_{max}$ , and by increasing  $E_{min}$  to 42 MeV, one still includes about 90% of the signal events. While more model-dependent, this increases the maximum detectable mass to about  $m_{max} = 14$  keV.

For comparison, we estimate how large  $m_{max}$  would be if the signal from neutrino-electron scattering were used. Since the signal is forward-peaked, the background can be substantially reduced with an angular cut. In this case, it makes sense to use the entire 32 kton volume. If 95% of the background can be removed, and the time-independent background rate of  $0.1 \text{ s}^{-1}$  used above for the inner 22.5 kton can be used for the full volume, then  $B \approx 0.005 \text{ s}^{-1}$ . Assuming that no signal events are lost with this cut, the number of events for  $E_{min} = 5$  MeV is about  $N_S = 60$ . At the three-sigma level, the maximum detectable mass is about  $m_{max} = 2$  keV, comparable to the estimate in Ref. [10].

If the  $\nu_\tau$  events appear to be missing, a large-mass search as above can be made. If nothing is found, there are three possibilities. The first possibility is that the mass is greater than 10 keV or so, and that it is stable over the time it takes to travel from the supernova, about  $3 \times 10^4$  years. Then its signal is so dispersed that it cannot distinguished against the background. However, as pointed out in Ref. [8], any neutrino with a mass greater than 10 keV or so would likely decay in such a time (this avoids violation of the cosmological bound on the neutrino masses, see Ref. [4] and references therein). The second possibility is that the mass was large enough that the neutrinos decayed, and that their decay products were not detected. The third possibility is that the  $\nu_\tau$  neutrino was not produced in the supernova, or at least significantly differently than expected. For example, if the  $\nu_\tau$  temperature were much lower than 8 MeV, there would be essentially no  $\nu_\tau$  events detected. These three possibilities cannot be distinguished without additional evidence.

## V. CONCLUSIONS AND DISCUSSION

One of the key points of our technique is that the abundant  $\bar{\nu}_e$  events can be used to calibrate the neutrino luminosity of the supernova and to define a clock by which to measure the delay of the  $\nu_x$  neutrinos. The internal calibration very substantially reduces the model dependence of our results. The measurement of time relative to the  $\bar{\nu}_e$  signal allows us to be sensitive to rather low masses. Without such a clock, one cannot determine a mass limit with the  $\langle t \rangle$  technique advocated here, since the absolute delay is unknown. Instead, one would have to constrain the mass from the observed dispersion of the events. Our calculations indicate that while a significant delay can be seen for  $m = 50$  eV, the dispersion does not become significant until  $m = 150$  eV or greater.

We first assumed that one of  $\nu_\mu$  and  $\nu_\tau$  masses was nonzero, and the other negligibly small. For convenience, we referred to the heavier one as  $\nu_\tau$ , though it is impossible to tell the difference. The results are given in Figs. 2 and 3. If it were known that the masses were almost degenerate, than a stricter limit can be placed. Those results are given in Figs. 4 and 5. If nothing more is known, the most conservative thing to do is to take the one-mass limit for each of  $\nu_\tau$  and  $\nu_\mu$ . As shown in Table III, if no statistically significant difference of the Reference and Signal is seen one can put an upper limit of 45 eV if one assumes that only one mass in nonvanishing, and 35 eV if one assumes that both  $\nu_\mu$  and  $\nu_\tau$  are massive (and that the masses are the same).

Given the large statistics of the  $\nu_x$  signal used here, one might wonder why the time delay is not larger and the mass sensitivity is not lower than we report here. The  $\nu_x$  average energy is about 25 MeV. For  $E \approx 25$  MeV,  $m = 50$  eV and  $D = 10$  kpc, the delay is about 2 s. However, from Eq. (10), what matters for the event rate is the peak of the product  $f(E)\sigma(E)$ . Since the cross section for the  $^{16}\text{O}$  excitation is very steep in energy, the peak energy is large, about 60 MeV. For  $E \approx 60$  MeV,  $m = 50$  eV and  $D = 10$  kpc, the delay is about 0.4 s. In both cases, these delays are for about 1/3 of the events in the Signal, so for a large integration time  $t_{max}$  the difference  $\langle t \rangle_S - \langle t \rangle_R$  would be about 1/3 of these delays. For moderate  $t_{max}$ , as used in the main analysis, the shift is slightly smaller (though more significant than for a larger  $t_{max}$ ).

These considerations show that the delay is reduced, and the statistical significance decreased, by the seemingly irreducible background of the  $\bar{\nu}_e$  events at low energies as well as by the background caused by the massless  $\nu_\mu$ . Besides, since the energy of the outgoing neutrino cannot be measured (or even the excitation energy in  $^{16}\text{O}$ ), it is not possible to measure the energy spectrum of the  $\nu_\tau$  neutrinos. Thus the  $\nu_x$  temperature can only be constrained from the total number of events.

The situation can be contrasted with the  $\bar{\nu}_e$  mass limit of about 20 eV from SN1987A established with only a

handful of events and no independent clock. There, however, it was possible to determine the incoming neutrino energy on the event by event basis, and to compare the neutrino energies versus time to the theoretical expectation. Moreover, the SN1987A was at about 50 kpc, compared to the 10 kpc assumed for the next Galactic supernova, and a lower typical energy should be used in the delay formula of the detected  $\bar{\nu}_e$  events than for the  $\nu_x$  neutral current scattering on  $^{16}\text{O}$ .

Some of the important parameters used here are not well known, though were treated as such. However, once there is actually a supernova, the model uncertainties will be greatly reduced by the  $\bar{\nu}_e$  data. For example, the binding energy  $E_B$  and the  $\bar{\nu}_e$  temperature will be determined. Other questions that can be resolved include the time dependence of the temperature, and whether a one-parameter thermal spectrum is sufficient to describe the energy spectra. Once a supernova is observed, the technique presented here can easily be run with the new parameters or necessary modifications. Second, for small changes in some parameters, the mass sensitivity does not change much. Note that this is especially true if mass is unrecognizably small, and we are making a limit.

The results of this paper are valid for either Dirac or Majorana neutrinos. We only considered stable neutrinos. The effects of decaying neutrinos on mass limits from supernovae are discussed in Ref [8]. We also considered unmixed neutrinos. Vacuum oscillations among  $\nu_\tau$ ,  $\nu_\mu$ , and their antiparticles are irrelevant since the numbers of neutrinos of each flavor are assumed to be equal. Vacuum oscillations between  $\nu_\tau$  and  $\nu_e$  or  $\nu_\mu$  and  $\nu_e$  and their antiparticles should have an observable effect on the  $\bar{\nu}_e$  spectrum. Oscillations to sterile neutrinos would also have an effect. The effects of either vacuum or matter-enhanced neutrino mixing on the neutrino signals are considered in, e.g., Ref. [22].

In conclusion: We have presented a rather general method, including a thorough statistical analysis, of extracting information about the possible  $\nu_\tau$  and  $\nu_\mu$  masses from the future detection of a Galactic supernova neutrino burst by the SuperKamiokande detector. When such an event in fact occurs, the existing mass limits will be vastly improved and will approach, or cross over, the cosmological bound.

## ACKNOWLEDGMENTS

This work was supported in part by the US Department of Energy under Grant No. DE-FG03-88ER-40397. J.F.B. was supported by a Sherman Fairchild fellowship from Caltech. We thank H.A. Bethe, B.W. Filippone, and Y.-Z. Qian for discussions.

- 
- [1] H.A. Bethe, Rev. Mod. Phys. **62**, 801 (1990).
- [2] S.E. Woosley, et al., Astrophys. J. **433**, 229 (1994).
- [3] H.-T. Janka, in *Vulcano Workshop 1992: Frontier Objects in Astrophysics and Particle Physics*, F. Giovanelli, G. Mannocchi, eds. (Italian Physical Society, 1993).
- [4] G.G. Raffelt, *Stars as Laboratories for Fundamental Physics* (University of Chicago Press, 1996), Ch. 7.
- [5] A.I. Belesev, et al., Phys. Lett. B **350**, 263 (1995).  
In fact, the measured value of  $m_{\bar{\nu}_e}^2$  is negative. Under the assumption  $m_{\bar{\nu}_e}^2 = 0$ , a Bayesian analysis gives  $m_{\bar{\nu}_e} \lesssim 5$  eV; see Ref. [6] for further discussion. For our purposes, the exact number used in the limit is less important than the fact that it is small.
- [6] R.M. Barnett, et al., Phys. Rev. D **54**, 1 (1996).
- [7] S. van den Bergh, Comments Astrophys. **17**, 125 (1993);  
G.A. Tammann, W. Löffler, A. Schröder, Astrophys. J. Suppl. **92**, 487 (1994).
- [8] J.M. Soares, L. Wolfenstein, Phys. Rev. D **40**, 3666 (1989).
- [9] D. Seckel, G. Steigman, T.P. Walker, Nucl. Phys. B **366**, 233 (1991).
- [10] L.M. Krauss, et al., Nucl. Phys. B **380**, 507 (1992).
- [11] A. Burrows, D. Klein, R. Gandhi, Phys. Rev. D **45**, 3361 (1992).
- [12] G. Fiorentini, C. Acerbi, Astropart. Phys. **7**, 245 (1997).
- [13] A. Acker, S. Pakvasa, R.S. Raghavan, Phys. Lett. B. **238**, 117 (1990).
- [14] D.B. Cline, et al., Phys. Rev. D **50**, 720 (1994).
- [15] P.F. Smith, Astropart. Phys. **8**, 27 (1997).
- [16] K. Langanke, P. Vogel, E. Kolbe, Phys. Rev. Lett. **76**, 2629 (1996).
- [17] Y. Takeuchi, Moriond Electroweak Workshop (March 1997);  
K. Inoue, TAUP Workshop (September 1997);  
Y. Totsuka, Texas Symposium (December 1996).
- [18] E. Kolbe et al., Nucl. Phys. A **540**, 599 (1992).
- [19] W.C. Haxton, Phys. Rev. D **36**, 2283 (1987).
- [20] Y. Totsuka, Rep. Prog. Phys. **55**, 377 (1992).
- [21] J.N. Bahcall, P.I. Krastev, E. Lisi, Phys. Rev. C **55**, 494 (1997).
- [22] Y.-Z. Qian, G.M. Fuller, Phys. Rev. D **49**, 1762 (1994).